Journal of Materials Chemistry A

Accepted Manuscript

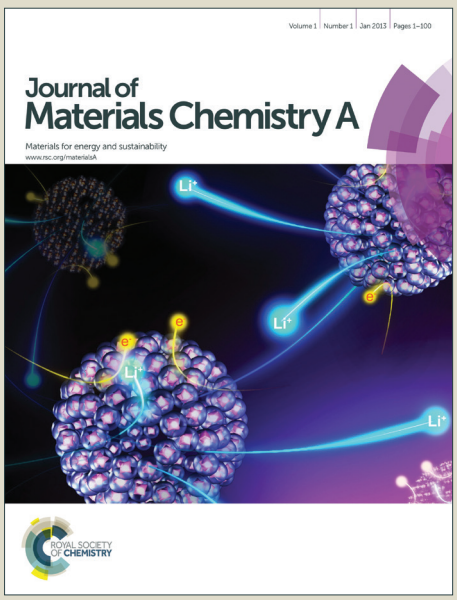

ROYAL SOCIETY OF CHEMISTRY

www.rsc.org/materialsA

Journal of Material Chemistry A

ARTICLE

Electrochemical behaviour of activated carbons obtained via hydrothermal carbonization

Received 00th January 20xx,
Accepted 00th January 20xx

DOI: 10.1039/x0xx00000x

www.rsc.org/

David Salinas-Torres,[a] Dolores Lozano-Castelló,[a] Maria Magdalena Titirici,[b,c] Li Zhao,[d] Linghui Yu,[e] Emilia Morallón [f] and Diego Cazorla-Amoros*[a]

Activated carbons were prepared by chemical activation with KOH of hydrochars obtained by hydrothermal carbonisation (HTC) using low cost and abundant precursors such as rye straw and cellulose. Hydrochars derived from rye straw were chemically activated using different KOH/precursor ratios, in order to assess the effect of this parameter on their electrochemical behaviour. In the case of the cellulose, the influence of the hydrothermal carbonisation temperature was studied by fixing activating agent/cellulose ratio. Furthermore, N-doped activated carbons were synthesised by KOH activation of hydrochars prepared by HTC from a mixture of glucose with melamine or glucosamine. In this way, N- doped activated carbons were prepared in order to evaluate the influence of the nitrogen groups in their electrochemical behaviour in acidic medium. The results showed that parameters such as the chemical activation or carbonisation temperature clearly affect the capacitance, since these parameters play a key role in the textural properties of the activated carbons. Finally, symmetric capacitors based on activated carbon and N-doped activated carbon were tested at 1.3 V in a two-electrode cell configuration and the results revealed that the N-groups improved the capacitance at high current density.

Introduction

Biomass derived carbons have attracted considerable interest due to the fact that the fossil resources, such as crude oil, natural gas and coal are scarce and generate large amounts of green house gases. Renewable and low-cost biomass is proposed as an environmentally sustainable solution for green energy in the future. Biomass can generate either bioenergy (i.e. biofuels) or materials for renewable energy devices.

As the amount of electricity generated from renewable but discontinuous sources such as solar and wind is constantly increasing, energy storage devices become more and more important. At this point, electrochemical double layer capacitors (EDLC) or supercapacitors offer a low-cost and efficient solution to high power density energy storage, while the limiting factor still remains the energy density. As materials are at the very core of improved performance, countless efforts have focused on the development of suitable materials to be used in these devices.

As previously stated, the main requirement of capacitors in the future is related to the improvement of the energy density without diminishing their typical power density and long-cycle life values. Several strategies are being developed to enhance the energy density values, which can be sorted out according to the optimization of the device configuration or the development of the electrode material. On the one hand, the optimisation of the configuration is focused on increasing the cell voltage. In this sense, hybrid systems are under constant research and a large number of materials are being subject of study, such as metal oxides (RuO_2 or MnO_2) [1,2] or conducting polymers (PANI or PEDOT) [3,4]. However, carbon materials are still the most used in the assembly of novel hybrid systems, as for example lithium-ion capacitors or nanohybrid capacitors [5–7]. For this reason, new strategies in synthesis of carbon materials are being developed in order to tailor their porosity to match the size of the electrolyte ions [8] as well as the tuning of the surface chemistry [9]. Many of the strategies followed used biomass or its byproducts as carbon materials precursor, due to biomass sources show high availability and rapid renewability. Moreover, biomass-derived porous carbons showed interesting electrochemical properties, which are similar to activated carbons, carbon nanotubes, activated carbon fibres and graphene [10,11].

Biomass-derived carbons can be prepared by different methods, such as pyrolysis [10], chemical/physical activation [11–13] and so on. Advanced carbon materials were synthesized from different kinds of biomass (seaweed,

[a] Departamento de Química Inorgánica e Instituto Universitario Materiales, Universidad de Alicante, E-03080 Alicante, Spain. E-mail: cazorla@ua.es
[b] Queen Mary University of London, School of Engineering and Materials Science, Mile End Road, E14NS, London
[c] Queen Mary University of London, Materials Research Institute, Mile End Road, E14NS, London
[d] National Center for Nanoscience and Technology, No.11, Beiyitiao Zhongguancun Beijing, 100190, China
[e] School for Engineering of Matter, Transport and Energy, Arizona State University, Tempe, AZ, 85287, USA
[f] Departamento de Química Física e Instituto Universitario de Materiales, Universidad de Alicante, Ap. 99 E-03080, Alicante, Spain
† Footnotes relating to the title and/or authors should appear here.
Electronic Supplementary Information (ESI) available: [details of any supplementary information available should be included here]. See DOI: 10.1039/x0xx00000x

eucalyptus wood, coconut shell, etc.) using different synthetic methods above-mentioned. Nevertheless, the hydrothermal carbonization was claimed as an alternative to obtain carbon materials, due to its low cost, mild synthesis conditions and environmentally friendly manufacture. Hence, biomass derived HTC carbons were considered as very promising materials for being used in supercapacitors [11,14–17].

The HTC method may provide carbon materials with better properties than those displayed by those derived from other synthetic routes. For example, chemical activation usually leads to a narrow pore size distribution (PSD) that may not be appropriate, whereas some reports showed that HTC leads to carbon materials with well-balanced micro- and mesoporosity and a good control of PSD [14,18]. HTC also offers the possibility of combining with hard- and soft-templating method or chemical activation to achieve suitable porous texture [11,19–21]. Another feature is that HTC-derived carbons usually exhibit high amount of oxygen functional groups [11,22] because the process is performed under mild conditions, maintaining most of the precursor initial oxygen content. This important result can be applied to other heteroatom-containing precursors, what led to the preparation of N-doped carbons by using the HTC method [15,23] which contained a higher nitrogen amount than those prepared by the conventional methods. Moreover, it was demonstrated that this high nitrogen amount prevails even after the chemical activation. It is known that nitrogen groups change the electrochemical properties, such as electron-donor character, conductivity and capacitance behavior [9,24–26]. The improvement of these electrochemical properties together with the control of the porous texture, would give suitable carbon materials to enhance the capacitors performance.

In the present study activated carbons obtained from hydrochars (synthesised from biomass, D-glucose and cellulose) were electrochemically characterised in aqueous electrolyte in a three-electrode cell by carrying out cyclic voltammetry and galvanostatic charge-discharge experiments. The effect of the activating agent/precursor ratio and the precursor origin on the electrochemical behaviour was studied.

Moreover, N-doped highly microporous carbons were prepared by chemical activation of a N-containing precursor hydrochar under same conditions used in the literature [27]. These N-doped carbons were tested in a three-electrode cell in aqueous media and subsequently, symmetric capacitors consisting of N-doped carbon and its analogous without nitrogen content were checked in a maximum cell voltage of 1.3 V in acid media in order to analyze the effect of nitrogen on the capacitor performance.

Although biomass-derived carbon materials prepared via hydrothermal carbonization followed by chemical activation have been previously reported in the literature, there is no study which clearly show the strong influence of the chemical activation ratio and carbonisation temperature on the capacitance of the material. Therefore this study will help understand the importance of the textural and structural parameters for an optimal performance as electrodes in supercapacitors.

Experimental

Materials

Some of the HTC-derived carbons using different precursors (D-glucose, cellulose, D-glucosamine and melamine) were prepared following the experimental conditions described previously [27-29]. Afterwards, chemical activation with KOH of HTC-derived carbons was performed using the procedure described in our previous works [27,30] with a KOH/precursor ratio of 3/1. In the case of hydrochars obtained from rye straw, the hydroxide/precursor ratios of 2/1, 3/1 and 4/1 (wt%) were used in order to analyse the effect of this ratio in the properties of the activated materials.

The samples were denoted as (X-Y ºC), being "X" the precursor (RS: rye straw, C: cellulose, G: glucose, G-mel: glucose + melamine, GA: glucosamine) and "Y" the carbonization temperature. Moreover, "h", "2", "3" or "4", was added at the end of the sample name to indicate that the sample was not activated (hydrochar) or was activated using 2:1, 3:1 or 4:1 hydroxide/precursor ratio, respectively.

Electrochemical and physicochemical characterisation

Elemental chemical analysis was performed in a (C, N, H) LECO analyser (Micro TruSpec model). X-ray photoelectron spectroscopy (XPS) measurements were performed using a K-Alpha spectrometer (Thermo-Scientific), which operates with a radiation Mg Kα, hυ = 1253.6 eV. Peak areas were estimated by fitting with a combination of Gaussian functions. Temperature-programmed desorption (TPD) experiments were performed in a DSC-TGA equipment (TA; SDT 2960 Simultaneous) coupled to a mass spectrometer (Balzers, OmniStar) to estimate the oxygen surface groups. The experimental conditions were as follows: heating rate of 20 ºC min^{-1} up to 940 ºC under helium flow rate of 100 ml min^{-1}.

Porous texture of the KOH-activated materials was characterised by physical adsorption of N_2 (−196 ºC) and CO_2 (0 ºC), using an automatic adsorption system (Autosorb-6, Quantrachrome). BET surface area, the total micropore volume (VN_2-DR) and narrow micropore volume (size < 0.7 nm) (VCO_2-DR) were calculated according to the conditions explained in the literature [31–33].

The electrochemical characterisation of the different electrodes was carried out using a standard three-electrode cell configuration. Reversible hydrogen electrode (RHE) was used as reference electrode and a spiral of platinum wire was employed as a counter electrode. 0.5 M H_2SO_4 solution was used as aqueous electrolyte. Cyclic voltammetry and galvanostatic charge/discharge cycling were the electrochemical techniques used. Regarding the capacitors, they were also assessed in a two-electrode cell using a sandwich type construction with a nylon membrane between

the electrodes. Gold disc was used as current collector and 0.5 M H_2SO_4 solution was used as electrolyte. The values of specific capacitance were determined by galvanostatic charge/discharge and they were referred to the total weight of the active mass of both electrodes. For the electrode preparation, the carbon material was mixed with the binder polytetrafluoroethylene (PTFE, 60 wt%) and acetylene black (Strem Chemicals) in a 85:5:10 wt% ratio. The electrochemical measurements were carried out with an EG&G Potentiostat/Galvanostat model 273 controlled by software ECHEM M270 and an Autolab PGSTAT302 with SCANGEN.

Results and discussion

Physicochemical characterisation

Characterisation of porous texture and surface chemistry. Fig. 1 shows the N_2 adsorption isotherms of activated carbons from glucose and N-containing glucoses, which are of type I, characteristic of microporous materials.

Attending to N_2 volume uptakes, it can be concluded that KOH activation led to an effective development of porosity, since the BET surface area and pore volume values calculated (Table 1) are much higher than those displayed by their precursors (A_{BET} ~20 $m^2\ g^{-1}$). Furthermore, surface area values of samples containing N (GA-180ºC-3 and Gmel-180ºC-3) are smaller than G-180ºC-3.

Activated carbons derived from rye straw and cellulose present N_2 adsorption isotherms similar to activated carbons from glucose-containing precursors (Fig. 2.a and b). Fig. 2.a contains the isotherms corresponding to RS-240ºC after KOH activation using different KOH/precursor ratio. Analogously to the behaviour observed for other precursors (lignocellulosic materials and coals) [30,34], in the case of hydrochars a KOH/precursor ratio increase also produces an increase in the porosity development.

Table 1. Porous texture corresponding to activated carbons from glucose and N-glucoses.

Sample	A_{BET}	VN_2-DR	VCO_2-DR
	$m^2\ g^{-1}$	$cm^3\ g^{-1}$	$cm^3\ g^{-1}$
G-180 ºC-3	1766	0.79	0.49
GA-180 ºC-3	1238	0.56	0.39
Gmel-180 ºC-3	1400	0.58	0.38

For the series of samples prepared from cellulose hydrothermally carbonized at different temperatures (Fig. 2.b.), the highest porosity development is observed for the C-240ºC-3 sample (A_{BET} = 2250 m^2/g). However, C-280ºC-3 shows the lowest porosity development (A_{BET} = 891 m^2/g), which indicates a lower degree of activation. Moreover, from the PSD obtained from N_2 adsorption (QSDFT) and CO_2 adsorption (NLDFT) (see Fig. S1 and S2 in the supporting information) it can be said that high hydrothermal carbonization temperature (e.g. 280 ºC) generates activated carbon with a lower porosity development and narrower PSDs, whilst the ones, produced at 180–240 ºC, upon KOH

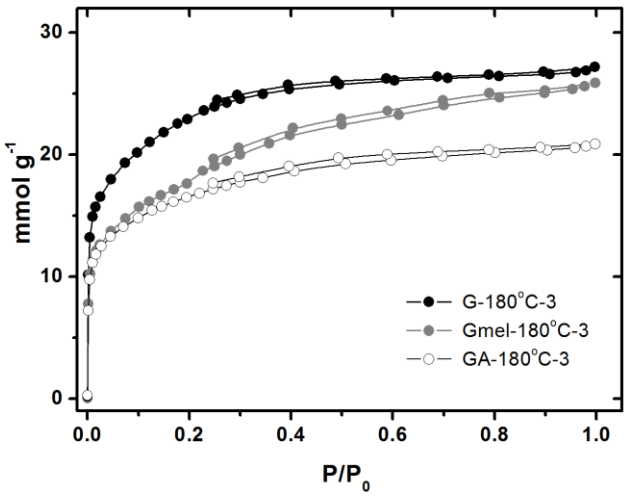

Fig. 1 N_2 adsorption isotherms of activated carbons from glucose and N-glucoses.

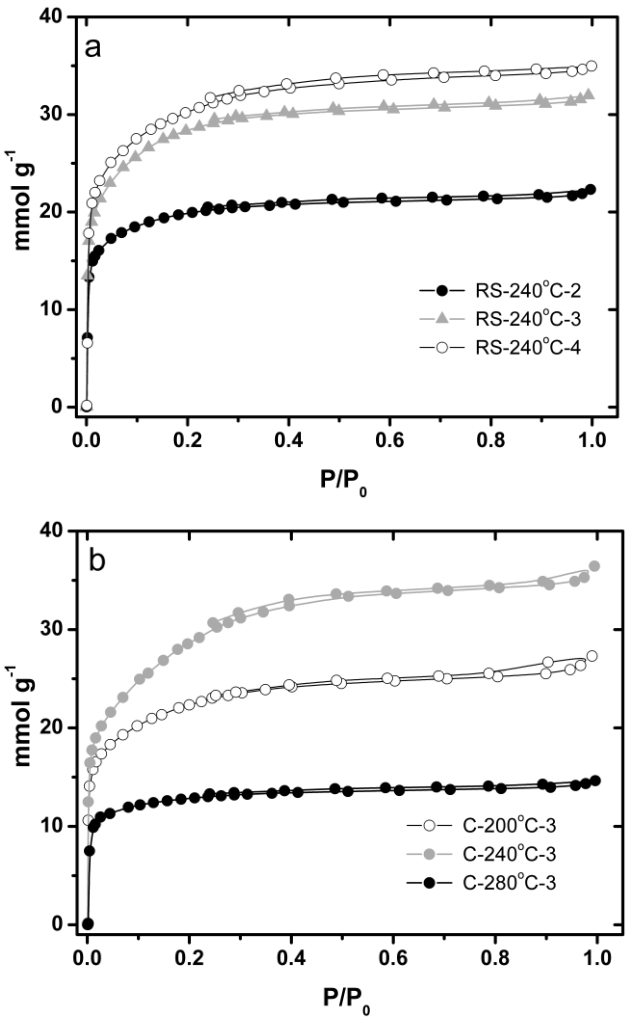

Fig. 2 (a) N_2 adsorption isotherms of ACs derived from rye straw and (b) and cellulose hydrochars

activation, develop a greater porosity characterized by a wider PSD [27].

Temperature programmed desorption experiments (TPD) were carried out in order to obtain information about the amount of surface groups. Fig. 3 shows CO and CO_2 profiles of activated carbons RS-240ºC-3, C-240ºC-3 and G-180ºC-3 as representative examples of each precursor.

The CO_2 and CO profiles present a similar trend for all samples. On the one hand, gases evolved as CO_2 are related to the decomposition of the acidic groups, such as carboxylic groups, lactones or anhydrides [35–37]. It can be observed that for all samples, the carboxylic groups (~300 ºC) and anhydrides (~450 ºC) showed the highest contribution, while they did not present a high content of lactones (>700 ºC).

The evolution of CO, which corresponds to the decomposition of basic/neutral and weakly acidic groups, (such as phenols, ethers and carbonyls [35–37]), was different for the studied samples, since RS-240ºC-3 exhibited a higher contribution of phenol groups (~600–700 ºC) than C-240ºC-3 and G-180ºC-3 samples.

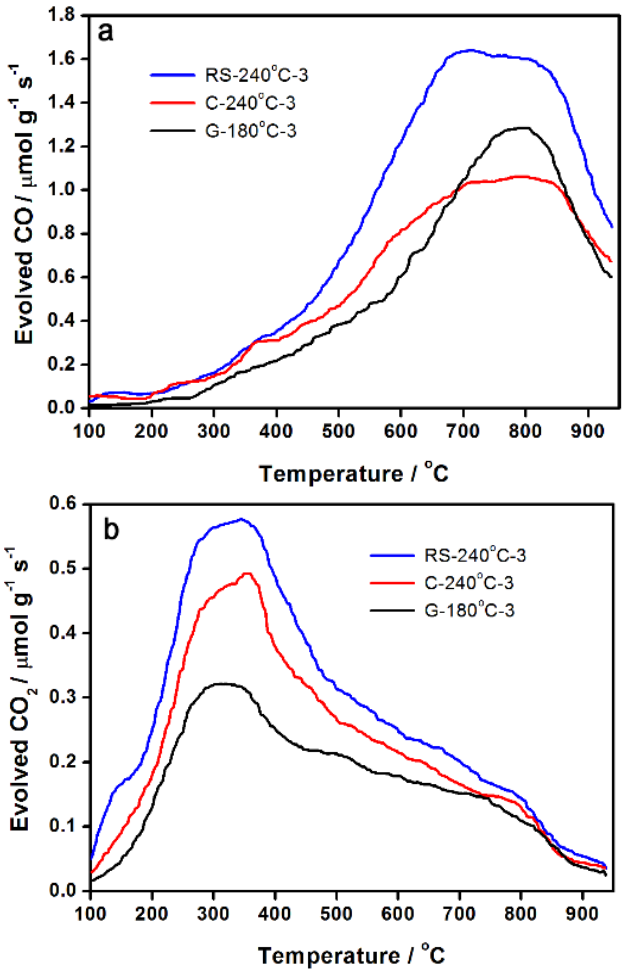

Fig. 3 (a) CO and (b) CO_2 TPD evolution profiles obtained from activated carbons derived from different precursor hydrochars.

In addition, all samples showed a high content of quinone groups (~700–900 ºC) [36], which are related to the pseudocapacitance [37–39].

Table 2 includes the quantification of the oxygen surface functionalities, which corresponds to the evolved amounts of CO and CO_2. As mentioned above, these materials have high amounts of CO-type groups (carbonyl, phenolic and anhydrides in a lower extent).

The total oxygen content increased when the KOH/precursor ratio was 4:1 with respect to 3:1 or 2:1 for rye straw samples. In the case of cellulose (Table 2) and glucose (results not shown here) the total oxygen content corresponding to the activated carbons synthesized at the highest temperature (C-280ºC-3 and G-240ºC-3) are much higher than those obtained at lower temperature (240 ºC or 200ºC). These results point out the importance of the structural differences in HTC materials depending on the hydrothermal carbonization temperature and the type of precursors, which was discussed in detail in our previous work [27].

Concerning the activated carbons derived from N-containing glucose, the TPD profiles analysis is not straightforward, since the oxygen groups which decompose as CO and CO_2 appear at the same range of temperature as the nitrogen groups.

Elemental analysis and X-ray photoelectron spectroscopy (XPS). Table 3 summarises the elemental composition of the activated carbons as well as their hydrochars. The elemental composition of ACs synthesised via chemical activation of biomass derived HTC carbons (rye straw and cellulose) are included in the supporting information (Table S1 in the supporting information).

XPS data of GA-180ºC-3 and Gmel-180ºC-3 show similar nitrogen content for both samples (~3.5 wt. %). This content is very close to those obtained by elemental analysis. This fact could indicate that nitrogen is well-distributed in the bulk of the materials.

Table 2. Quantification of oxygen surface groups from TPD experiments and capacitance values.

Sample	CO	CO_2	O	C [b]
	µmol g^{-1}	µmol g^{-1}	µmol g^{-1}	F g^{-1}
RS-240ºC-2	2055	891	3837	207
RS-240ºC-3	2028	704	3436	228
RS-240ºC-4	3337	1109	5595	234
C-200 ºC-3	1587	603	2793	181
C-240 ºC-3	1401	570	2541	191
C-280 ºC-3	2239	811	3861	182
G-180 ºC-3	1311	424	2159	175
GA-180 ºC-3 [a]	2790	940	4670	186
Gmel-180 ºC-3 [a]	2697	1255	5207	162

(a) This amount is not only related to oxygen surface functionalities because N-functionalities also decompose at the same range of temperatures. (b) Values obtained at 1mV s-1.

Table 3. Elemental analysis (EA) and XPS characterisation of hydrochars and activated carbons.

Sample	EA	XPS		
	wt% N	wt% N	wt% C	wt% O
G-180ºC-h	0.0	0.0	74.2	25.8
GA-180ºC-h	--	5.7	77.0	17.3
Gmel-180ºC-h	--	42.5	39.8	17.7
G-180ºC-3	0.0	0.0	81.2	18.8
GA-180ºC-3	2.7	3.5	78.6	17.9
Gmel-180ºC-3	3.1	3.4	69.1	27.5

The nitrogen content measured by XPS shows a different trend for the studied samples. In the case of sample Gmel-180ºC-h, the nitrogen content decreases drastically when Gmel-180ºC-h was chemically activated (from 42.5 to 3.4 wt% N), while this decrease is not very important for the glucosamine sample.

Therefore, the different behaviour of N-hydrochars when they are activated under the same experimental conditions can be attributed to several parameters, such as the different chemical stability of surface groups.

Fig. 4.a and c show XPS spectra for N-hydrochars. It can be observed that GA-180ºC-h and Gmel-180ºC-h show two peaks. The first peak, at low binding energies, is centred at around 399.7 eV and corresponds to amine groups [40], which is more intense in the case of the Gmel-180ºC-3 (~70 % of amine groups) than GA-180ºC-3 (~54 % of amine groups). The second peak in the case of GA-180ºC-h sample appears at about 401.8 eV, and it can be assigned to quaternary N groups. However, for Gmel-180ºC-h sample the second peak at 400.9 eV, can be assigned to pyridone/pyrrole. However, XPS spectra of activated samples (GA-180ºC-3 and Gmel-180 ºC-3, Fig. 4 b and d) show two peaks, a main peak at binding energies close but higher than 400 eV and a small one centred at around 399.3 eV, which are related to positively charged N-functionalities

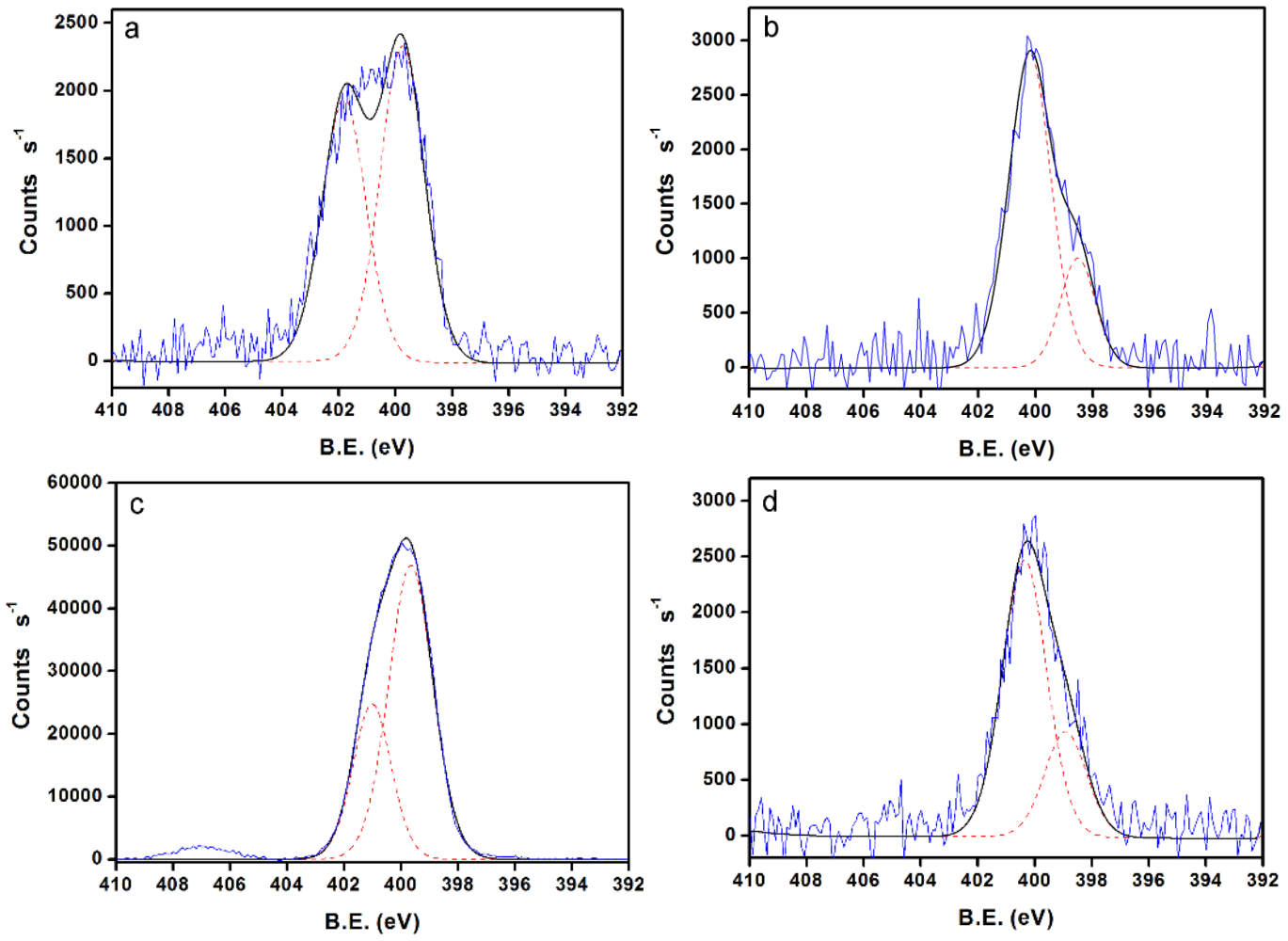

Fig. 4. N1s XPS spectra: a) GA-180ºC-h, b) GA-180ºC-3 (activated sample), c) Gmel-180ºC-h and d) Gmel-180ºC-3 (activated sample).

like pyridone/pyrrole and pyridine groups, respectively [40]. XPS analysis of samples after the activation process showed the same kind of nitrogen groups for all the studied samples, while the nitrogen peaks assignment was different in the hydrochars. The similarities between the N-containing activated carbons revealed that Gmel-180ºC-h had a great amount of amine groups, which are removed at around 600 ºC, as it was previously reported elsewhere [41]. The changes observed from the hydrochars to the activated carbons are a consequence of condensation reactions that favour the formation of graphene domains with N-species located at the edges of the graphene layers or inside the layer. In this last case, if pyridines or pyrroles are located in the graphene layer, vacancies are formed that create additional edge sites. Interestingly, for these N-containing activated carbons only two kinds of N-functionalities are formed and no peak at around 402 eV appears, what indicates that the amount of quaternary N species is very small. Usually, N-doping in porous carbons using other experimental approaches produce materials with a significant amount of quaternary N species. Thus, pyridone/pyrrole and pyridine groups are the main species what will allow us to get fundamental information about the influence of these species in the electrochemical behaviour.

Electrochemical characterisation

Effect of the chemical activation ratio. As it was previously mentioned in the experimental section, rye straw precursor was carbonized by hydrothermal carbonization method at 240 ºC. Subsequently, RS-240ºC-h was chemically activated with KOH for different activating agent/precursor ratios. All activated carbons were tested in a standard three-electrode cell in acidic solution (0.5 M H_2SO_4).

Fig. 5 shows the voltammograms of the ACs derived from rye straw in acidic medium. The voltammograms between 0 and 0.8 V exhibits quasi-rectangular shape, indicating that the main contribution to the capacitance is the charge and discharge of the electrical double layer. Nevertheless, a small peak at around 0.65 V during the positive scan and its counter-process at around 0.5 V during the negative scan are observed. This redox processes is associated to surface oxygen groups of the activated carbon that contribute to the pseudocapacitance [37,38].

Regarding to the effect of the chemical activation ratio in the capacitance, a slightly increase in the capacitance is observed when the activating agent/precursor ratio increases from 2:1, 3:1 to 4:1, obtaining 207, 228 and 234 F g^{-1}, respectively (see Table 2). It is worth mentioning that the capacitance value for RS-240ºC-h was around 1 F g^{-1} as consequence of its low porosity. The apparent surface areas for RS-240ºC-3 and RS-240ºC-4 are around 2200 m^2 g-1 while RS-240ºC-2 presents a value around 1500 m^2 g^{-1} [27]. Therefore, these values confirm that the major contribution to capacitance is due to the surface area, since RS-240ºC-2 and RS-240ºC-3 samples have a similar amount of oxygen groups (obtained by TPD experiments), but the capacitance value for RS-240ºC-2 sample is lower than for RS-240ºC-3 sample (see Table 2).

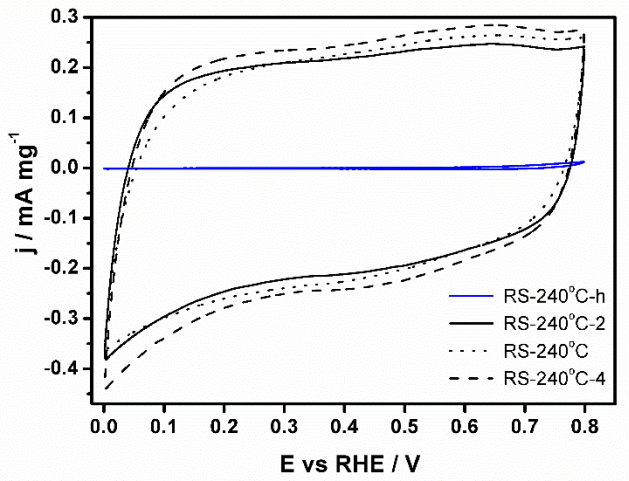

Fig. 5 Steady voltammograms for the carbon materials obtained from rye straw precursor in a 0.5 M H_2SO_4 solution. Scan rate 1 mVs^{-1}.

Table 4 shows the capacitance values for activated carbons obtained from galvanostatic experiments at different current densities. The chronopotentiograms have a triangular shape as corresponds to a capacitive behaviour (Fig. S3 and S4 in the supporting information). It can be observed that the capacitance decreases for all samples when current density increases, which is associated to the ion diffusion problems inside the pores due to high micropore volume of the ACs derived from rye straw. The capacitance values are comparable with those values obtained from biomass precursors in the literature [11] and the capacitance retention is very high reaching a value around 50% of the initial value at 1 A g^{-1}. Taking into account the results presented in this section, it can be concluded that these materials are suitable as electrode in supercapacitors.

Influence of the carbonisation temperature. In this section, the influence of the carbonisation temperature during the hydrothermal process on the electrochemical properties was assessed. Cellulose hydrochars were prepared at 200 ºC, 240 ºC and 280 ºC and they were electrochemically characterised in a three-electrode cell. Fig. 6 shows the electrochemical behaviour of C-200ºC-3, C-240ºC-3, C-280ºC-3 activated carbons and a cellulose hydrochar (C-240ºC-h).

Table 4. Specific capacitance obtained from galvanostatic experiments at different current densities (three-electrode cell).

	C / F g^{-1}		
j / mA g^{-1}	RS-240ºC-2	RS-240ºC-3	RS-240ºC-4
25	353	426	441
100	295	342	354
250	261	299	319
500	219	256	275
750	196	228	248
1000	179	208	229

The cyclic voltammograms show a significant increase of the current for the activated carbons compared to the cellulose hydrochar.

The voltammograms also present quasi-rectangular shape, similar to the activated carbons derived from rye straw. However, the redox processes related to the existence of oxygen groups are not clearly distinguished. Concerning the capacitance values (see Table 2), C-240ºC-3 showed higher capacitance value than C-200ºC-3 and C-280ºC-3, which is related to a higher surface area of sample C-240ºC-3 (A_{BET} = 2250 m^2 g^{-1}). Additionally, C-200ºC-3 and C-280ºC-3 showed similar capacitance values, but the surface area of C-200ºC-3 (A_{BET} = 1642 m^2 g^{-1}) is twice the A_{BET} of C-280ºC-3 (A_{BET} = 891 m^2 g^{-1}). Thus, this similarity in the capacitance value when the surface area is so different and the absence of peaks mentioned above, would indicate that the capacitance value of C-280ºC-3 can be related to the effective electrosorption of ions inside the pores smaller than 1 nm [8], since, as it was discussed above, the PSD of C-280ºC revealed that its average pore size was below 1.5 nm while the C-200ºC-3 and C-240ºC-3 presented a wider micropore size distribution with micropores larger than 1.5 nm (Fig. S1 and S2 in the supporting information). In the case of C-240ºC-3 the voltammogram shows a more rectangular shape indicating that the diffusion at the limit potentials is improved with respect to the other samples. This can be associated with the wider pore size distribution for this sample having an important contribution of narrow mesopores that can facilitate ion diffusion.

The galvanostatic charge-discharge experiments (Fig. S5 in the supporting information) exhibited the same trend as the activated carbon derived from rye straw. According to the data obtained, it can be concluded that carbonization temperature during hydrothermal process affects to the porous texture of activated carbon, modifying its electrochemical behaviour.

Effect of nitrogen content in the capacitor performance. As it was previously mentioned, surface groups play an important role in the electrochemical properties of carbon materials. The most common surface groups in carbon materials are oxygen groups. However, heteroatoms such as nitrogen, phosphorous and sulphur are also important. For this reason, the effect of nitrogen content on the capacitor performance was studied.

The role of the nitrogen groups in the capacitor performance is still being studied in the current literature. It has been observed that nitrogen groups had influence on the capacitor performance in organic media [42]. However, Hulicova et al. studied the nitrogen effect in the electrochemical properties in acidic media. It was pointed out that pyridinic nitrogen and pyrrolic nitrogen were the most effective in a double layer formation while quaternary-N and pyridinic-N-oxides improved the capacitance due to their positive charge [43]. Moreover, the nitrogen groups showed an enhancement in the capacitance in neutral and basic electrolytes [15, 26, 44].

Firstly, the samples previously mentioned (G-180ºC-3, GA-180ºC-3 and Gmel-180ºC-3) were characterised in a three-electrode cell in aqueous solution (0.5 M H_2SO_4). The voltammograms display quasi-rectangular shape corresponding to capacitive behaviour (Fig. 7). Moreover, the presence of some overlapped peaks at around 0.45–0.65 V can be related to the existence of oxygen and nitrogen groups, which were confirmed by XPS experiments.

Table 5 contains the capacitance values for G-180ºC-3, GA-180ºC-3 and G-mel-180ºC-3, which were obtained from galvanostatic charge-discharge experiments. It can be observed that capacitance values are very similar for the three samples. However, the surface areas for N-doped carbons are lower than G-180ºC (see Table 1). Therefore, the presence of surface nitrogen groups contributes to the capacitance.

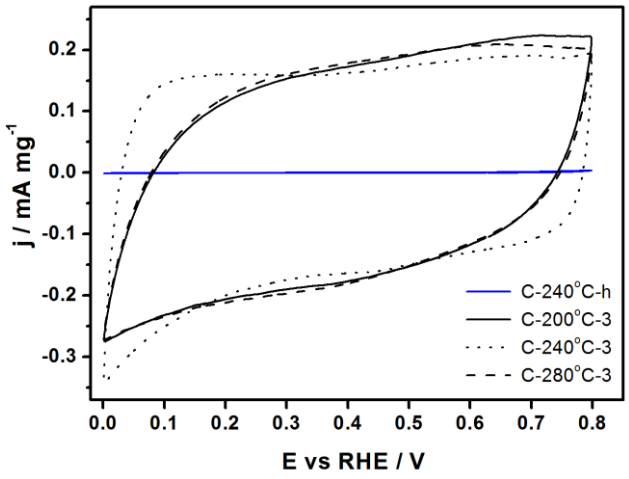

Fig. 6 Steady state voltammograms for the cellulose sample (carbonized) and activated carbons derived from cellulose in a 0.5 M H_2SO_4 solution. Scan rate 1 mVs^{-1}.

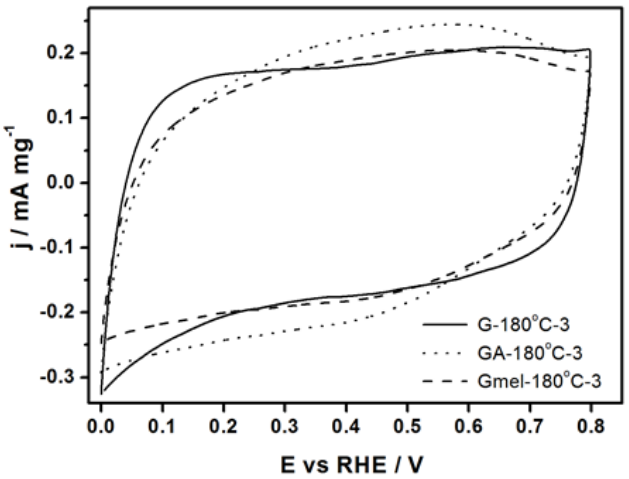

Fig. 7 Steady voltammograms for activated carbons derived from glucose in a 0.5 M H_2SO_4 solution. Scan rate 1 mVs^{-1}.

Table 5. Capacitance values obtained from galvanostatic experiments at different current densities (three-electrode cell).

	C / F g^{-1}		
j / mA g^{-1}	G-180ºC-3	GA-180ºC-3	Gmel-180ºC-3
25	280	287	253
100	235	226	197
250	194	184	161
500	159	145	130
750	136	120	108
1000	117	100	91

From the results shown in this section, G-180ºC-3 and GA-180ºC-3 samples were selected to assemble symmetric capacitors, which were tested in acidic solution.

Symmetric capacitor based on ACs derived from glucose. Symmetric capacitors were prepared using G-180ºC-3 and GA-180ºC-3 as electrodes and 0.5 M H_2SO_4 as electrolyte. The cell used was a sandwich-type configuration. These symmetric capacitors were tested by galvanostatic charge-discharge experiments in a maximum cell voltage of 1.3 V, in order to evaluate the effect of the nitrogen in the capacitance performance. The capacitance values were referred to the weight of the total active mass of the capacitor.

Fig. 8 shows the chronopotentiograms at 500 mA g^{-1} for the two capacitors in a potential window of 1.3 V. The chronopotentiogram of the G-180ºC-3/G-180ºC-3 capacitor showed a quasi-triangular shape, indicating the absence of faradic processes. However, the symmetric GA-180ºC-3/GA-180ºC-3 capacitor presents a slight deviation of this shape, which is associated to the pseudofaradic processes [45].

The presence of a pseudocapacitive contribution was also observed for the GA-180ºC-3 in a three-electrode cell, confirming that the surface nitrogen groups of the GA-180ºC-3 sample contribute to the pseudocapacitance. The capacitance of GA-180ºC-3/GA-180ºC-3 capacitor presented values lower than the G-180ºC-3/G-180ºC-3 capacitor. However, when the current density increases the values are similar for both capacitors despite the lower A_{BET} of the GA-180ºC-3 sample.

The evolution of the gravimetric capacitance with the current density for the G-180ºC-3/ G-180ºC-3 and GA-180ºC-3/GA-180ºC-3 capacitors is shown in Fig. 8b. Both symmetric capacitors showed an important decrease in the capacitance value when the current density increased. This decrease in the capacitance when the current density increases was more pronounced for the G-180ºC-3 / G-180ºC-3 capacitor than for the GA-180ºC-3 / GA-180ºC-3 capacitor. The capacitance drop is related to the diffusivity limitations for ions to form the double layer in the microporosity. Therefore, the presence of surface nitrogen groups seems to facilitate the charge transfer at high current density.

Fig. 9 shows the evolution of the gravimetric capacitance versus the number of charge-discharge cycles for both symmetric capacitors.

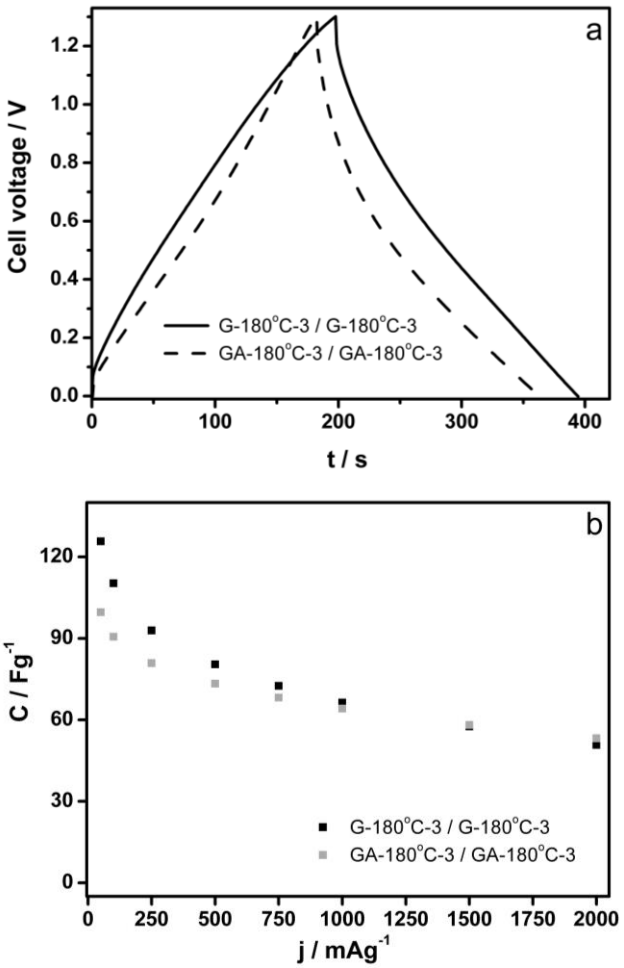

Fig. 8 (a) Galvanostatic charge-discharge experiments for the G-180ºC-3 / G-180ºC-3 and GA-180ºC-3 / GA-180ºC-3 capacitors at 500 mAg^{-1}. (b) Capacitance variation with the current density for the G-180ºC-3 / G-180ºC-3 and GA-180ºC-3 / GA-180ºC-3 capacitors operated at 1.3 V of potential window. Two-electrode cell configuration; 0.5 M H_2SO_4.

It can be observed that the gravimetric capacitance decreases with the number of cycles being the GA-180ºC-3 capacitor the one that suffers a lower decrease. However, they retained more than 90 % of the initial capacitance after 1000 cycles at 1.3 V.

In order to achieve a complete view of the performance of both symmetric capacitors, the specific power (P) and specific energy (E) were obtained from the following equations [46]:

$$P = \frac{V^2}{4.ESR.m_t} \qquad E = \frac{1}{2}.C.V^2$$

Table 6 summarises the energy density and power density values obtained for both symmetric capacitors in a potential window of 1.3 V. The specific energy for the symmetric G-180ºC-3/G-180ºC-3 capacitor was 8.9 Wh kg^{-1}, which is slightly higher than that displayed by symmetric GA-180ºC-3/GA-180ºC-3 capacitor.

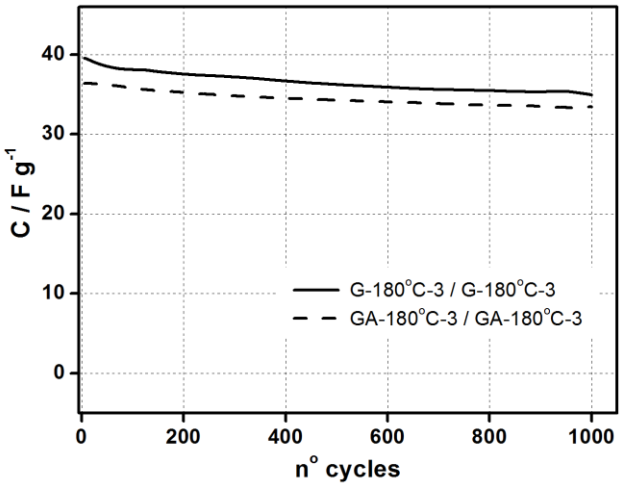

Fig. 9 Evolution of the capacitance versus the number of cycles for the G-180ºC-3 / G-180ºC-3 and GA-180ºC-3 / GA-180ºC-3 capacitors at 1.3 V in 0.5 M H_2SO_4. Charge/discharge current density 500 mA g^{-1}. Two-electrode cell configuration.

However, GA-180ºC-3/GA-180ºC-3 capacitor presented higher volumetric energy density than the symmetric G-180ºC-3/G-180ºC-3 capacitor, which constitutes an important benefit from a practical point of view. The specific energy obtained with these capacitors are higher than those values achieved using supercapacitors based on activated carbons with high surface area [10]. The specific power is similar for both capacitors showing a better performance the capacitor prepared with the GA-180ºC-3 sample.

In view of these results, activated carbons derived from the glucose and glucosamine are promising materials as electrodes, to be used in electrochemical capacitors. Moreover, the addition of heteroatoms improved the capacitor performance in volumetric basis and when expressed per surface area. The XPS measurements show that the N-containing activated carbons contain mainly pyrrole/pyridone and pyridine groups, being the former in a higher concentration (Fig. 4). Quaternary-N species are negligible.

Then, the results obtained confirm the beneficial contribution of pyridone and pyridine groups due to pseudocapacitance [24,26] and of pyrrole groups since they improve the electron mobility and electron transfer reactions of the carbon matrix through introduction of electron-donor properties [47], what may explain the higher retention of capacitance observed for the N-containing materials.

Table 6. Power density and energy density obtained at 1.3 V in 0.5 M H_2SO_4

Capacitor	*Pmax*		*E*	
	kW kg^{-1}	kW dm^{-3}	W h kg^{-1}	W h dm^{-3}
G-180ºC-3/G-180ºC-3	2.3	0.5	8.9	2.0
GA-180ºC-3/GA-180ºC-3	2.6	0.8	8.6	2.5

Therefore, the hydrothermal carbonization combined with the chemical activation is an adequate procedure to obtain activated carbons with remarkable porosity development, and adequate surface chemistry which are suitable for being used in supercapacitors.

Conclusions

Activated carbons derived from biomass, cellulose and glucose were electrochemically characterised in acidic medium. It can be concluded that the chemical activation ratio and carbonisation temperature have an important effect in the capacitance of the material. This is due to the fact that these parameters strongly influence the textural properties of the activated carbons. Moreover, the presence of nitrogen groups improved both the capacitance and charge transfer mainly at high current density.

Symmetric capacitors were assembled and assessed in acidic media for the potential window of 1.3 V, obtaining energy density values comparable to symmetric capacitors based on activated carbons with high surface area. Moreover, the symmetric capacitor based on GA-180ºC sample, which contains nitrogen, showed an improvement in volumetric energy density and a good cycle-life test after 1000 charge-discharge cycles at 500 mA g^{-1}. The results confirm the influence of pyridine and pyridone groups in pseudocapacitance and of pyrrole groups in favouring the electron mobility through the graphene layers.

Acknowledgements

The authors thank the Spanish MINECO, GV and FEDER (PROMETEOII/2014/010, Projects CTQ2012-31762 and MAT2013-42007-P) and D.S.T. is indebted to MINECO for a pre-doctoral FPI grant (BES-2010-035238). M. Titirici, Li Zhao and Linghui Yu would like to acknowledge financial support from the Max-Planck Society. Li Zhao is grateful to China Scholarship Council for awarding her a PhD fellowship in Germany.

Notes and references

1 C. Sassoye, C. Laberty, H. Le Khanh, S. Cassaignon, C. Boissière, M. Antonietti and C. Sanchez, *Adv. Funct. Mater.*, 2009, **19**, 1922.
2 V. Khomenko, E. Raymundo-Piñero and F. Béguin, *J. Power Sources*, 2006, **153**, 183.
3 D. Salinas-Torres, J. M. Sieben, D. Lozano-Castelló, D. Cazorla-Amorós and E. Morallón, *Electrochim. Acta*, 2013, **89**, 326.
4 G. A. Snook, P. Kao and A. S. Best, *J. Power Sources*, 2011, **196**, 1.
5 K. Naoi, S. Ishimoto, Y. Isobe and S. Aoyagi, *J. Power Sources*, 2010, **195**, 6250.
6 T. Aida, K. Yamada and M. Morita, *Electrochem. Solid-State Lett.*, 2006, **9**, A534.

7 X. Sun, X. Zhang, H. Zhang, N. Xu, K. Wang and Y. Ma, *J. Power Sources*, 2014, **270**, 318.
8 J. Chmiola, G. Yushin, Y. Gogotsi, C. Portet, P. Simon and P. L. Taberna, *Science*, 2006, **313**, 1760.
9 M. Seredych, D. Hulicova-Jurcakova, G. Q. Lu and T. J. Bandosz, *Carbon* , 2008, **46**, 1475.
10 E. Raymundo-Piñero, M. Cadek and F. Béguin, *Adv. Funct. Mater.*, 2009, **19**, 1032.
11 C. Falco, J. M. Sieben, N. Brun, M. Sevilla, T. Van Der Mauelen, E. Morallón, D. Cazorla-Amorós and M.-M. Titirici, *ChemSusChem*, 2013, **6**, 374.
12 L. M. Cotoruelo, M. D. Marqués, A. Leiva, J. Rodríguez-Mirasol and T. Cordero, *Adsorption*, 2011, 17, 539.
13 J. Wang and S. Kaskel, *J. Mater. Chem.*, 2012, **22**, 23710.
14 Y. Fan, X. Yang, B. Zhu, P.-F. Liu and H.-T. Lu, *J. Power Sources*, 2014, **268**, 584.
15 M. Sevilla, W. Gu, C. Falco, M. M. Titirici, A. B. Fuertes and G. Yushin, *J. Power Sources*, 2014, **267**, 26.
16 L. Wei, M. Sevilla, A. B. Fuertes, R. Mokaya and G. Yushin, *Adv. Energy Mater.*, 2011, **1**, 356.
17 H. Zhu, X. Wang, F. Yang and X. Yang, *Adv. Mater.*, 2011, **23**, 2745.
18 D. Puthusseri, V. Aravindan, B. Anothumakkool, S. Kurungot, S. Madhavi and S. Ogale, *Small*, 2014, **10**, 4395.
19 S. Kubo, R. J. White, N. Yoshizawa, M. Antonietti and M.-M. Titirici, *Chem. Mater.*, 2011, **23**, 4882.
20 S. Kubo, R. J. White, K. Tauer and M.-M. Titirici, *Chem. Mater.*, 2013, **25**, 4781.
21 M.-M. Titirici, A. Thomas and M. Antonietti, *Adv. Funct. Mater.*, 2007, **17**, 1010.
22 M. Sevilla, a. B. Fuertes and R. Mokaya, *Energy Environ. Sci.*, 2011, **4**, 1400.
23 R. J. White, M. Antonietti and M.-M. Titirici*, J. Mater. Chem.*, 2009, **19**, 8645.
24 D. Hulicova-Jurcakova, M. Kodama, S. Shiraishi, H. Hatori, Z. H. Zhu and G. Q. Lu, *Adv. Funct. Mater.*, 2009, **19**, 1800.
25 D. Hulicova, M. Kodama and H. Hatori, *Chem. Mater.*, 2006, **18**, 2318.
26 O. Ornelas, J. M. Sieben, R. Ruiz-Rosas, E. Morallón, D. Cazorla-Amorós, J. Geng, N. Soin, E. Siores and B. F. G. Johnson, *Chem. Commun.*, 2014, **50**, 11343.
27 C. Falco, J. P. Marco-Lozar, D. Salinas-Torres, E. Morallón, D. Cazorla-Amorós, M. M. Titirici and D. Lozano-Castelló, *Carbon*, 2013, **62**, 346.
28 N. Brun, S.A. Wohlgemuth, P. Osiceanu and M.M. Titirici, Green Chem., 2013, **15**, 2514.
29 R.J. White, M. Antonietti and M.M. Titirici, J. Mater. Chem., 2009, **19**, 8645.
30 D. Lozano-Castelló, M. A. Lillo-Ródenas, D. Cazorla-Amorós and A. Linares-Solano, *Carbon*, 2001, 39, 741.
31 D. Cazorla-Amorós, J. Alcaniz-Monge and A. Linares-Solano, *Langmuir*, 1996, **12**, 2820.
32 D. Cazorla-Amorós, J. Alcañiz-Monge, M. A. De La Casa-Lillo and A. Linares-Solano, *Langmuir*, 1998, **14**, 4589.
33 D. Lozano-Castelló, D. Cazorla-Amorós and A. Linares-Solano, *Carbon*, 2004, **42**, 1231.
34 A. Linares-Solano, D. Lozano-Castelló, M.A. Lillo-Ródenas and D. Cazorla-Amorós, Chemistry and Physics of Carbon, 2008, **Vol. 30**, 1-62.
35 M. C. Román-Martínez, D. Cazorla-Amorós, A. Linares-Solano and C. S.-M. de Lecea, *Carbon*, 1993, **31**, 895.
36 J. L. Figueiredo, M. F. R. Pereira, M. M. A. Freitas and J. J. M. Órfão, *Carbon*, 1999, **37**, 1379.
37 M. J. Bleda-Martínez, D. Lozano-Castelló, E. Morallón, D. Cazorla-Amorós and A. Linares-Solano, *Carbon*, 2006, **44**, 2642.
38 C.-T. Hsieh and H. Teng, *Carbon*, 2002, **40**, 667.
39 M. J. Bleda-Martínez, J. A. Maciá-Agulló, D. Lozano-Castelló, E. Morallón, D. Cazorla-Amorós and A. Linares-Solano, *Carbon*, 2005, **43**, 2677.
40 E. Raymundo-Piñero, D. Cazorla-Amorós, A. Linares-Solano, J. Find, U. Wild and R. Schlögl, *Carbon*, 2002, **40**, 597.
41 S. Kuroki, Y. Hosaka and C. Yamauchi, *Carbon*, 2013, **55**, 160.
42 D. Salinas-Torres, S. Shiraishi, E. Morallón and D. Cazorla-Amorós, *Carbon*, 2015, **82**, 205.
43 D. Hulicova-Jurcakova, M. Seredych, G. Q. Lu and T. J. Bandosz, *Adv. Funct. Mater.*, 2009, **19**, 438.
44 L. Zhao, L.-Z. Fan, M.-Q. Zhou, H. Guan, S. Qiao, M. Antonietti and M.-M. Titirici, *Adv. Mater.*, 2010, **22**, 5202.
45 E. Raymundo-Piñero, F. Leroux and F. Béguin, *Adv. Mater.*, 2006, 18, 1877.
46 A. G. Pandolfo and A. F. Hollenkamp, *J. Power Sources*, 2006, **157**, 11.
47 V. Strelko, V. Kuts and P. Thrower, *Carbon*, 2000, **38**, 1499.

Journal of Materials Chemistry

ARTICLE

Text for Table of Contents

Porous carbons were synthesised using hydrochars from low cost precursors. Electrochemical behaviour is influenced by synthesis conditions and precursor used.

Electrochemical behaviour of activated carbons obtained via hydrothermal carbonization

David Salinas-Torres, Dolores Lozano-Castelló, Maria Magdalena Titirici, Li Zhao, Linghui Yu, Emilia Morallón and Diego Cazorla-Amorós